ASEAN
Journal of Scientific and Technological Reports
Online ISSN:2773-8752

Research article

Structural and Electrical Characteristics of $CaCu_{3-x}Fe_xTi_4O_{12}$ Ceramics

Pariwat Dumnui[1], Atittaya Changchuea[2], Marina Mani[3], Jakkree Boonlakhorn[4*], and Pornjuk Srepusharawoot[5]

[1] Faculty of Science and Digital Innovation, Thaksin University, Songkhla, 90000, Thailand
[2] Faculty of Science and Digital Innovation, Thaksin University, Songkhla, 90000, Thailand
[3] Faculty of Science and Digital Innovation, Thaksin University, Songkhla, 90000, Thailand
[4] Faculty of Science and Digital Innovation, Thaksin University, Songkhla, 90000, Thailand
[5] Faculty of Science, Khon Kaen University, Khon Kaen, 40002, Thailand
* Correspondence: jakkree.b@tsu.ac.th

Citation:
Dumnui, P.; Changchuea, A.; Mani, M.; Boonlakhorn, J.; Srepusharawoot, P. Structural and electrical characteristics of $CaCu_{3-x}FexTi_4O_{12}$. *ASEAN J. Sci. Tech. Report.* **2025**, *28*(2), e256400. https://doi.org/10.55164/ajstr.v28i2.256400.

Article history:
Received: October 19, 2024
Revised: January 25, 2025
Accepted: March 12, 2025
Available online: April 1, 2025

Publisher's Note:
This article is published and distributed under the terms of the Thaksin University.

Abstract: Fe^{3+} doped $CaCu_3Ti_4O_{12}$ ceramics were successfully synthesized using a ball-milling oxide approach. Introducing Fe^{3+} doping resulted in a refined microstructure, significantly reducing the mean grain size of the $CaCu_3Ti_4O_{12}$ ceramics. Dielectric property measurements were conducted at various temperatures. Increasing the Fe^{3+} content from 0 to 0.1 mol at room temperature led to a substantial decrease in dielectric permittivity, dropping from approximately 66246 to 435 at 10 kHz. This reduction in dielectric permittivity is closely associated with a substantial increase in grain resistance, which results in lower polarization density per volume and further contributes to the decline in dielectric permittivity. Additionally, low-frequency relaxation was observed at room temperature due to Fe^{3+} doping, likely attributed to grain boundary effects, specifically grain boundary relaxation. At elevated temperatures, the influence of grain boundaries in the doped ceramics becomes more pronounced than the extremely high grain resistance, leading to complete interfacial polarization and, thus, high dielectric permittivity within this temperature range. Furthermore, all Fe^{3+} doped $CaCu_3Ti_4O_{12}$ ceramics exhibited nonlinear J-E characteristics, with the breakdown electric field enhanced from 31 to 41 V/cm due to Fe^{3+} doping. Although the doping of Fe^{3+} into the $CaCu_3Ti_4O_{12}$ lattice does not enhance the energy storage properties due to the reduced permittivity at room temperature, the findings from this study provide crucial fundamental information. This knowledge will serve as a valuable foundation for researchers interested in developing $CaCu_3Ti_4O_{12}$ ceramics, enabling further advancements in applications for electronic devices, energy storage, or other advanced technologies in the future.

Keywords: $CaCu_3Ti_4O_{12}$; Doping; Microstructure; Impedance spectroscopy; Nonlinear J-E characteristics.

1. Introduction

The $CaCu_3Ti_4O_{12}$ (CCTO) perovskite ceramic has attracted significant interest recently. According to previous studies, CCTO exhibits an exceptionally high dielectric permittivity (ε′) ranging from 10^2 to 10^5. This property, its stability at high frequencies and temperatures, and its nonlinear electrical behavior make it a promising candidate for further investigation [1, 2]. These features are significant for applications in energy storage capacitors, sensors, and varistors [1, 2]. Nevertheless, the exact origin of giant permittivity remains unclear. In

perovskite materials, including ferroelectrics, huge permittivity is generally linked to ionic displacements within a noncentrosymmetric lattice structure [3]. Subramanian and his team reported that phase transitions cannot be induced in CCTO and structurally related oxides [4]. Therefore, ionic displacements may not be the main cause of the high ε′ observed in these materials. Some studies propose that the elevated ε′ in CCTO and similar structural oxides is due to interfacial polarization. This phenomenon occurs at the interfaces between grains and grain boundaries [5, 6], and in low-resistivity materials, it can also occur between the electrodes and the ceramics [7]. In addition to the previously reported findings, there is a suggestion that space charge polarization may also play a role in the high ε′ observed at low frequencies in CCTO ceramics [8]. Adams et al. [9] demonstrated the electrical heterogeneity of CCTO, identifying both semiconducting grains and insulating grain boundary regions. This observation is consistent with the electrical microstructure observed in internal barrier layer capacitors (IBLCs), explaining the giant dielectric behavior of CCTO ceramics. The findings presented provide empirical evidence supporting the extrinsic effects associated with the high ε′ of CCTO.

Introducing metal ions into the crystal lattice of CCTO and structurally related oxides can modify the electrical properties of both the grains and the grain boundaries, resulting in changes to the dielectric characteristics of these materials [6, 10-12]. Alterations in dielectric behavior can result from variations in the extrinsic microstructure, which includes factors such as grain size and grain boundary thickness. Additionally, intrinsic factors like the formation of oxygen vacancies (V_O) and charge compensation mechanisms, influenced by high-temperature sintering and doping processes, also play a significant role [6, 13]. Typically, Vo and charge compensation mechanisms are inherently linked and cannot be separated. To achieve charge equilibrium, it is essential to facilitate the transition of metal ions, particularly Cu and Ti, to different valence states, forming Cu^{+} and/or Ti^{3+} ions [6, 14]. Cu^{2+} and/or Ti^{3+} ions play a crucial role in forming n-type semiconductive grains within the grain structure of CCTO and related ceramics. This phenomenon is enhanced by the short-range movement of charge carriers between the Ti^{3+}-O-Ti^{4+} and Cu^{+}-O-Cu^{2+} ions. It is important to highlight that the density of charge carriers significantly affects changes in the ε′ [15]. As discussed earlier, the various types and concentrations of dopants can lead to alterations in the dielectric and electrical properties of ceramics with an IBLC structure, which can be attributed to variations in defects in the lattice structure [10-12]. Observing two or more dielectric relaxations has been reported in specific instances [16]. In addition to the previously discussed studies, the increased ε′ in CCTO-based ceramics can be ascribed to several additional factors. These factors encompass the effects of domain boundaries [17], capacitance mechanisms related to micro- and nanoscale barrier layers [18], and the existence of small insulating defect clusters [19]. Although an IBLC structure is generally recognized as the main contributor to the significant dielectric properties observed in CCTO-based ceramics, it is essential to consider the role of intrinsic properties as a crucial factor that should not be disregarded [14]. As noted in previous research reports, substituting identical ions at different positions within the lattice structure significantly affects the material's properties. For instance, doping Ge^{4+} in Cu^{2+} or Ti^{4+} positions and Sn^{4+} in the same positions leads to considerable variations in the structural and dielectric properties [20-23]. Specifically, introducing Ge^{4+} or Sn^{4+} at the Cu^{2+} sites reduces grain size, while substituting at the Ti^{4+} sites causes an increase in grain size [20-23]. Nevertheless, incorporating Sn^{4+} or Ge^{4+} into the CCTO lattice enhances the dielectric properties of this material. This is particularly evident in maintaining a high energy storage capability, as indicated by the high ε′ value while reducing the energy loss capability, as represented by the low loss tangent (tanδ) value. Investigations into the coordination number of Fe^{3+} have revealed that Fe^{3+} can occupy Cu^{2+} and Ti^{4+} sites within the CCTO lattice [24]. Previous studies have documented the incorporation of Fe^{3+} into these sites, with some focusing on the structural characteristics [25] and others examining the dielectric properties [26-28]. Notably, doping at different sites produces varying results. However, despite these insights, the nonlinear electrical properties of Fe^{3+}-doped CCTO remain unexamined. To address this gap and deepen the understanding of this material, this study investigates the structure, dielectric properties, and nonlinear electrical properties of Fe^{3+}-doped CCTO, specifically targeting doping at the Cu^{2+} site.

This study analyzes the structural, dielectric, and nonlinear electrical properties of $CaCu_{3-x}Fe_xTi_4O_{12}$ ceramics, where x=0, 0.05, and 0.10 mol. The effects of doping on the crystalline structure and microstructure were investigated in detail. Additionally, the influence of doping on the dielectric and nonlinear electrical properties was systematically examined. The following sections will present experimental details, results, and discussions.

2. Materials and Methods

The $CaCu_{3-x}Fe_xTi_4O_{12}$ (x=0, 0.05, and 0.10 mol) ceramics were synthesized via a ball-milling oxide approach, with initial raw oxides including Fe_2O_3 (99.9% purity), TiO_2 (99.9% purity), CuO (99.0% purity), and $CaCO_3$ (99.9% purity). The raw oxides were carefully weighed according to stoichiometric proportions and combined with C_2H_6O (99.95% purity) within PP bottles. Zirconia balls filled half of the PP bottles, after which milling commenced at 200 rpm for 1 day using a milling instrument. Subsequently, the mixed raw oxides were transferred to a beaker and dried in an oven at 100 °C until all liquids were evaporated. The resulting dried precursors were then crushed to a fine powder and subjected to calcination at 850 °C for 12 h. After calcination, the powders were ground to achieve a mostly uniform particle size. All calcined powders underwent a second calcination at 900 °C for 12 h, followed by another crushing round to ensure a smooth consistency. The $CaCu_{3-x}Fe_xTi_4O_{12}$ powders were formed into pellets with a thickness of 2.5 mm and a diameter of 9.5 mm. The pellet was sintered in a furnace at 1060 °C for 6 h using a heating rate of 5 °C per min. In this work, $CaCu_{3-x}Fe_xTi_4O_{12}$ ceramics with x=0, 0.05, and 0.10 mol are designated CCTO, CCTO-Fe05, and CCTO-Fe10 ceramics, respectively.

The microstructure and crystal structure of $CaCu_{3-x}Fe_xTi_4O_{12}$ ceramics were studied using the ThermoFisher Scientific, Model: Quattro-S E-SEM (FE-SEM) and the X-ray Powder Diffraction (XRD) Equipment: Bruker D8 Advance Model, respectively. The software used for analyzing the SEM and XRD results were ImageJ software and X'Pert HighScore Plus software, respectively. The dielectric properties and impedance spectroscopy were evaluated using a B&K Precision LCR Meter Model 895 and a temperature-controlled testing probe. The temperature and frequency used in the test were 30 °C to 270 °C and 10^2 to 10^6 Hz, respectively. At room temperature, the nonlinear current-density electric-field (J-E) characteristics were evaluated using a Precise S300 desktop source source measurement unit. The voltage was incrementally increased at a rate of 0.226 V/s. The calculation of dielectric properties and impedance spectroscopy has been completed. The relationship used in the calculation of ε′ is as follows:

$$\varepsilon' = C_p d / \varepsilon_0 A \quad (1)$$

C_p represents the relative capacitance obtained from the dielectric test, where d signifies the distance between parallel electrodes, A denotes the electrode's area, and ε_0 stands for the permittivity of free space. Impedance spectroscopy is a crucial approach to inspecting the electrical response of materials, especially IBLC structural oxides. Complex impedance ($Z^*=Z' - iZ''$) can be calculated using following equation:

$$\varepsilon^* = \varepsilon' - i\varepsilon'' = [i\omega C_0 (Z' - iZ'')]^{-1} \quad (2)$$

ε″ represents the total loss factor, calculated as $\varepsilon'' = \varepsilon' \times \tan\delta$, where tanδ is the loss tangent obtained from the dielectric test. Z′ and Z″ denote the real and imaginary parts of Z*, respectively. C_0 is the capacitance of free space, and ω is the angular frequency. The Z* spectra results can be utilized to ascertain the resistances of grains (R_g) and grain boundaries (R_{gb}) in IBLC structural oxides. The breakdown electric field (E_b) is the electric field strength at a one mA/cm2 J. The nonlinear coefficient (α) can be calculated over the range of J from 1 to 10 mA/cm² using the following equations.

$$\alpha = \log(J_2/J_1)/\log(E_2/E_1) \quad (3)$$

Here, E_1 and E_2 represent the electric fields associated with current densities J_1 = 1 mA/cm² and J_2 = 10 mA/cm², respectively.

3. Results and Discussion

The crystal structure analysis of Fe-doped CCTO ceramics is presented in Figures 1(a–d). As illustrated in Figure 1(a), the XRD patterns for CCTO, CCTO-Fe05, and CCTO-Fe10 ceramics show a pure crystalline structure consistent with that of CCTO, following the standard JCPDS No. 75–2188 pattern [4]. Notably, no significant impurity phases are observed in the XRD patterns. The XRD data were analyzed using the Rietveld refinement technique and compared with the standard structure of CCTO, as illustrated in Figures 1(b-d). The results show that the XRD data fit well with the model obtained from the Rietveld refinement. The parameters indicating the quality of the Rietveld analysis demonstrate excellent values, as presented in Table 1. The expected R-value (R_{exp}), profile R-value (R_p), and weighted profile R-value (R_{wp}) are all below 13%. Furthermore, the goodness-of-fit (GOF) factor is also highly favorable, ranging between 1.02 and 1.67. The

lattice parameters of CCTO, CCTO-Fe05, and CCTO-Fe10 ceramics, as determined through Rietveld refinement, are summarized in Table 1. Specifically, the lattice parameters for CCTO, CCTO-Fe05, and CCTO-Fe10 are 7.3920(1), 7.3936(1), and 7.3940(1) Å, respectively. Correspondingly, the unit cell volumes are calculated to be 403.91(2), 404.17(2), and 404.24(2) Å^3, respectively. These findings align closely with previously reported values for CCTO ceramics, supporting the reliability of the current data [4].

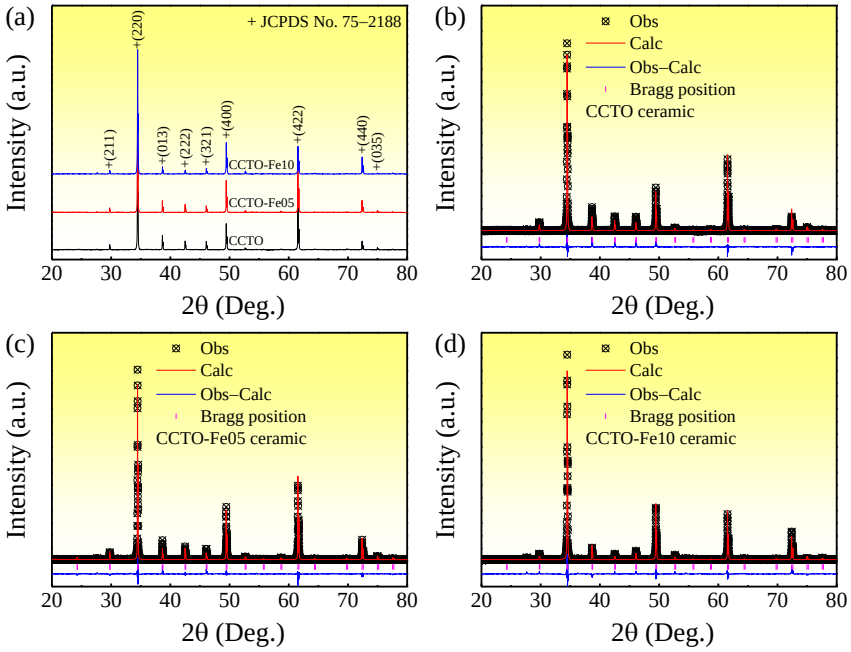

Figure 1. (a) XRD patterns of CCTO, CCTO-Fe05, and CCTO-Fe10 ceramics. (b-d) Rietveld refinement profiles for (b) CCTO, (c) CCTO-Fe05, and (d) CCTO-Fe10 ceramics.

Table 1. Structural parameters were obtained from XRD and SEM analyses for CCTO, CCTO-Fe05, and CCTO-Fe10 ceramics.

Sample	Structure	Space group	Cell parameters	Atoms	Atomic positions			GOF and R-factors	G (μm)
CCTO	*bcc*	*I m*3	a=7.3920(1) Å	Ca	0.0000	0.0000	0.0000	R_{exp}= 7.6202	5.46±0.98
		No. 204	V=403.91(2) Å^3	Cu	0.0000	0.5000	0.5000	R_p= 5.9590	
				Ti	0.2500	0.2500	0.2500	R_{wp}= 9.4624	
				O	0.0000	0.1798	0.3026	GOF=1.5420	
CCTO-Fe05	*bcc*	*I m*3	a=7.3936(1) Å	Ca	0.0000	0.0000	0.0000	R_{exp}= 10.0352	3.65±1.05
		No. 204	V=404.17(2) Å^3	Cu/Fe	0.0000	0.5000	0.5000	R_p= 7.6317	
				Ti	0.2500	0.2500	0.2500	R_{wp}= 10.1304	
				O	0.0000	0.1798	0.3026	GOF=1.0191	
CCTO-Fe10	*bcc*	*I m*3	a=7.3940(1) Å	Ca	0.0000	0.0000	0.0000	R_{exp}= 9.9951	3.83±0.87
		No. 204	V=404.24(2) Å^3	Cu/Fe	0.0000	0.5000	0.5000	R_p= 9.5558	
				Ti	0.2500	0.2500	0.2500	R_{wp}= 12.9317	
				O	0.0000	0.1798	0.3026	GOF=1.6739	

The SEM images depicting the surface microstructures and grain size distributions of CCTO, CCTO-Fe05, and CCTO-Fe10 ceramics are presented in Figures 2(a–c). The SEM images demonstrate that the grain sizes of all three ceramic materials exhibit a uniform fineness. Specifically, the average grain sizes of the CCTO-Fe05 and CCTO-Fe10 ceramics are marginally smaller than that of the CCTO ceramics. This observation suggests that incorporating Fe^{3+} into the lattice structure of CCTO effectively reduces grain size, even under identical temperature and time sintering conditions. After conducting calculations on the average grain sizes of the three ceramic materials, it was determined that the average grain sizes for CCTO, CCTO-Fe05, and CCTO-Fe10 ceramics were 5.46 ± 0.98, 3.65 ± 1.05, and 3.83 ± 0.87 μm, respectively. The reduction in grain size of Fe^{3+}-doped CCTO ceramics may result from the mismatch between the ionic radii of Fe^{3+} dopant ions and Cu^{2+} host sites. This mismatch induces lattice strain energy in the doped ceramics, which is attributed to the solute drag mechanism [29]. Consequently, the average grain size of the CCTO-Fe05 and CCTO-Fe10 ceramics decreases compared to that of the undoped CCTO sample.

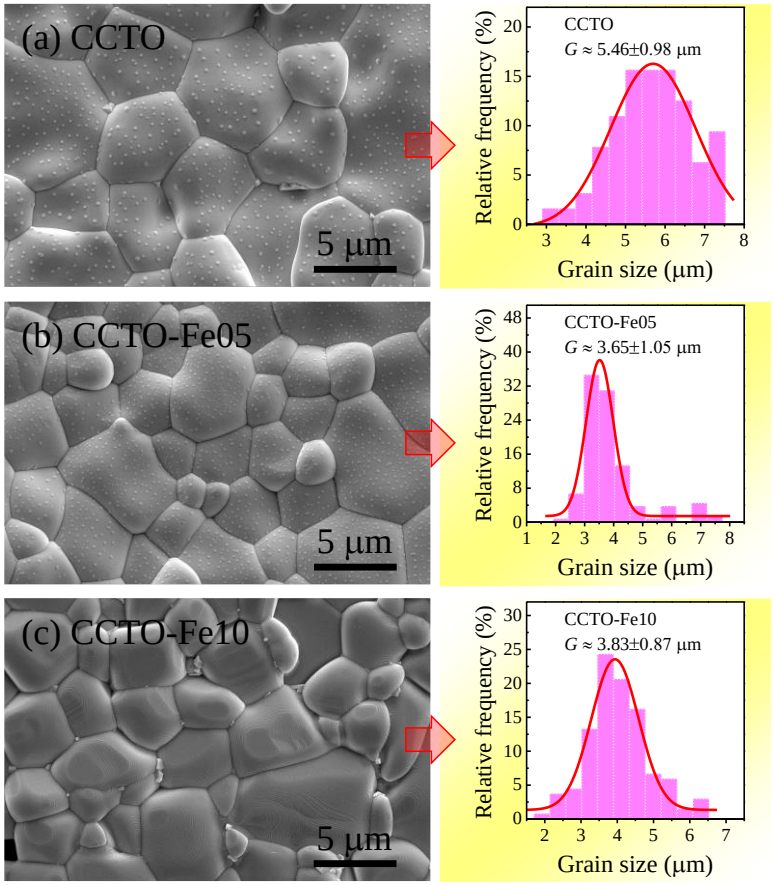

Figure 2. Surface microstructures and grain size distributions of (a) CCTO, (b) CCTO-Fe05, and (c) CCTO-Fe10 ceramics.

The frequency dependencies of ε′ and tanδ for CCTO, CCTO-Fe05, and CCTO-Fe10 ceramics at room temperature are presented in Figures 3(a) and 3(b), respectively. As shown in the Figure 3(a), the ε′ value of CCTO ceramic is the highest. However, after doping with Fe^{3+} at concentrations of x = 0.05 and x = 0.10 mol, the ε′ value significantly decreases, reducing by approximately two orders of magnitude. As listed in Table 2, at a frequency of 10 kHz, the ε′ values for CCTO, CCTO-Fe05, and CCTO-Fe10 ceramics are measured at 66246, 445, and 435, respectively. Materials characterized by an IBLC structure typically demonstrate a direct correlation between grain size and the ε′ value. In the case of the CCTO, CCTO-Fe05, and CCTO-Fe10 ceramics, it is observed that the grain size undergoes only a minor reduction, whereas the ε′ value exhibits a pronounced decrease, an atypical observation. This considerable decline in the ε′ value for CCTO-Fe05 and CCTO-Fe10 ceramics may be ascribed to alterations in intrinsic factors resulting from Fe^{3+} doping [26], which substantially

influences the ε′ value. According to previous research by Mu et al. [26], incorporating Fe^{3+} into the Ti^{4+} sites of the CCTO lattice significantly increases the R_g. This suggests a reduction in charge carriers within the grains, which decreases the density of polarization vectors per volume in the grains of CCTO material. As a result, the value of ε′ is markedly lower when compared to pure CCTO ceramic. As illustrated in Figure 3(b), the tanδ values of CCTO ceramics exhibit considerable stability within the frequency range of 10^2 to 10^4 Hz. In contrast, the tanδ values for CCTO-Fe05 and CCTO-Fe10 ceramics demonstrate a marked decrease with increasing frequency. This observation suggests that the incorporation of Fe^{3+} into the CCTO lattice facilitates low-frequency relaxation in the CCTO-Fe05 and CCTO-Fe10 ceramics. Prior research indicates that this low-frequency relaxation may be linked to the effects of DC conduction [30]. However, alternative factors, such as grain boundary effects, may also play a significant role in the observed low-frequency relaxation phenomenon. To ensure accuracy, it is essential to study the electrical properties of the samples using the impedance spectroscopy technique. If the observed results are due to DC conduction, the R_{gb} values for CCTO-Fe05 and CCTO-Fe10 ceramics should be significantly lower than those for the CCTO ceramic. As listed in Table 2, at a frequency of 10 kHz, the tanδ values for CCTO, CCTO-Fe05, and CCTO-Fe10 ceramics are measured at 0.059, 0.149, and 0.178, respectively.

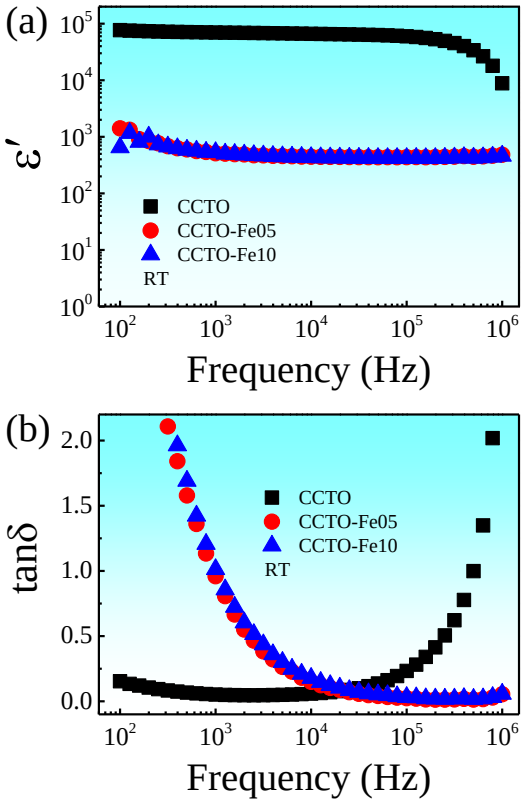

Figure 3. Frequency dependences of (a) ε′ and (b) tanδ at room temperature for CCTO, CCTO-Fe05, and CCTO-Fe10 ceramics.

Table 2. Room temperature measurements of grain resistance (R_g), grain boundary resistance (R_{gb}), dielectric permittivity (ε′) at 10 kHz, dielectric loss tangent (tanδ) at 10 kHz, breakdown electric field (E_b), and nonlinear coefficient (α) for CCTO, CCTO-Fe05, and CCTO-Fe10 ceramics.

Sample	R_g (Ω·cm)	R_{gb} (Ω·cm)	ε′	tanδ	E_b (V/cm)	α
CCTO	~50	~4.50×10^6	66246	0.059	33	3.35
CCTO-Fe05	-	~3.66×10^6	445	0.149	38	1.73
CCTO-Fe10	-	~3.38×10^6	435	0.178	41	1.17

In the investigation of the dielectric properties of CCTO, CCTO-Fe05, and CCTO-Fe10 ceramics across a broad temperature spectrum, as depicted in Figures 4(a-c), a notable increase in the ε′ values of all samples were observed with the elevation of the test temperature. This observed trend, presented in Figure 4(a) for the CCTO ceramic, correlates with a corresponding rise in the ε″ values illustrated in the inset. This behavior may be attributed to the mechanisms of DC conduction [30]. At 1 kHz, the value of ε′ increases approximately 3.90 times at 270 °C compared to room temperature for the CCTO ceramic. This change in ε′ can be attributed to the influence of DC conduction. At a frequency of 1 kHz, the increase in the ε′ value at 270 °C compared to room temperature is approximately 92 times for CCTO-Fe05 ceramics and 87 times for CCTO-Fe10 ceramics, respectively. The ε′ values at 270 °C for CCTO-Fe05 and CCTO-Fe10 ceramics are 47127 and 46391, respectively, which are comparable to the ε′ value of CCTO ceramics at room temperature. This suggests that, at elevated temperatures, the significant increase in ε′ may be attributed to interfacial polarization occurring at the grain boundaries of CCTO-Fe05 and CCTO-Fe10 ceramics. This phenomenon arises because charge carriers gain sufficient energy to overcome the resistance within the grains and migrate to the grain boundaries, resulting in an elevated ε′ value. Another possible factor contributing to the higher ε′ values of CCTO-Fe05 and CCTO-Fe10 ceramics is the influence of DC conduction; however, this effect is likely less pronounced than that of the grain boundary contributions.

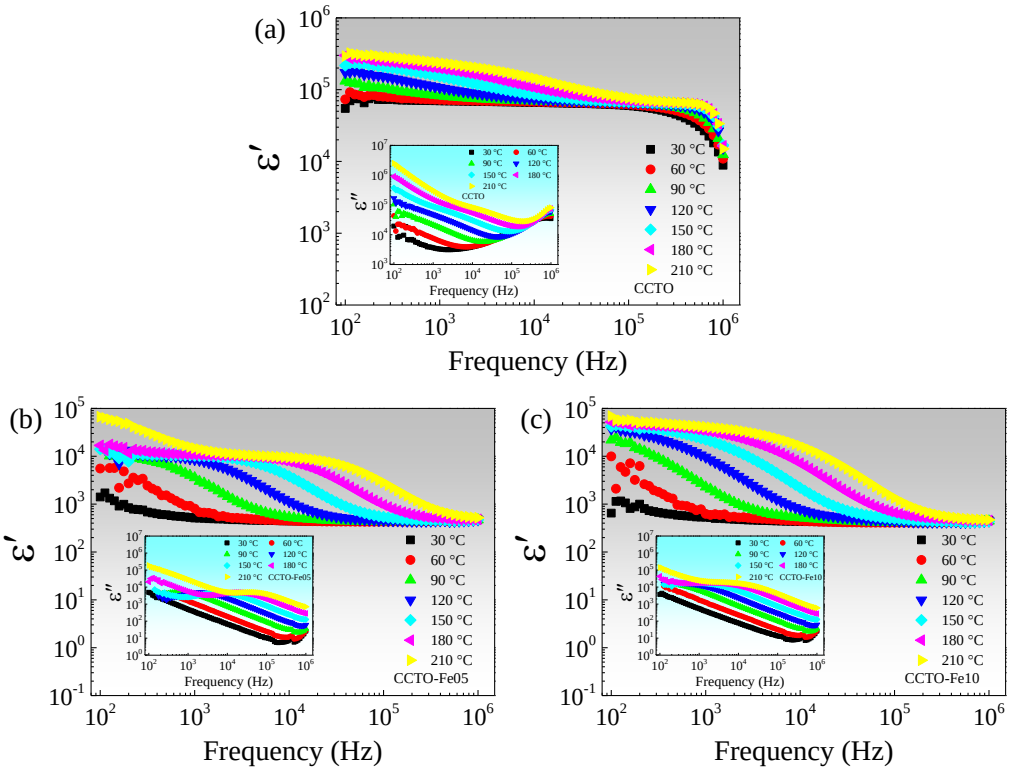

Figure 4. Frequency dependence of the real part of the ε′ for (a) CCTO, (b) CCTO-Fe05, and (c) CCTO-Fe10 ceramics at various temperatures. The insets show the corresponding frequency dependence of the ε″ for each ceramic.

The nonlinear electrical characteristics of CCTO, CCTO-Fe05, and CCTO-Fe10 ceramics were tested at room temperature, as illustrated in Figure 5. The results reveal a nonlinear relationship between the electric field (E) and the current density (J) in all tested samples. These J-E characteristics indicate that Fe^{3+} doped CCTO may exhibit an IBLC-like structure consistent with previous reports [31]. The test results also indicate that adding Fe to the CCTO lattice enhances the E_b of the material. As shown in Table 2, the E_b values for CCTO, CCTO-Fe05, and CCTO-Fe10 ceramics are 33, 38, and 41 V/cm, respectively. The α values for CCTO, CCTO-Fe05, and CCTO-Fe10 ceramics are 3.35, 1.73, and 1.17, respectively.

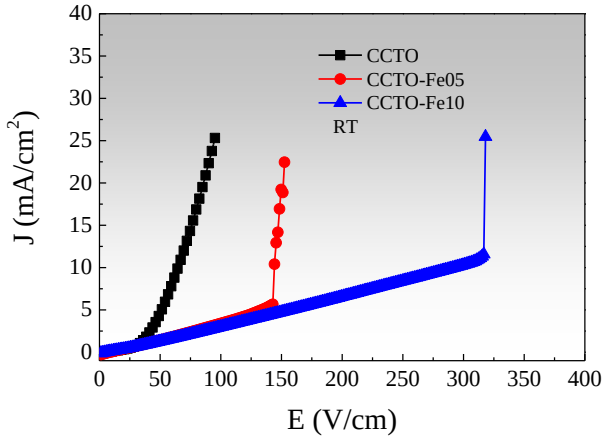

Figure 5. Nonlinear J-E characteristics at room temperature of CCTO, CCTO-Fe05, and CCTO-Fe10 ceramics.

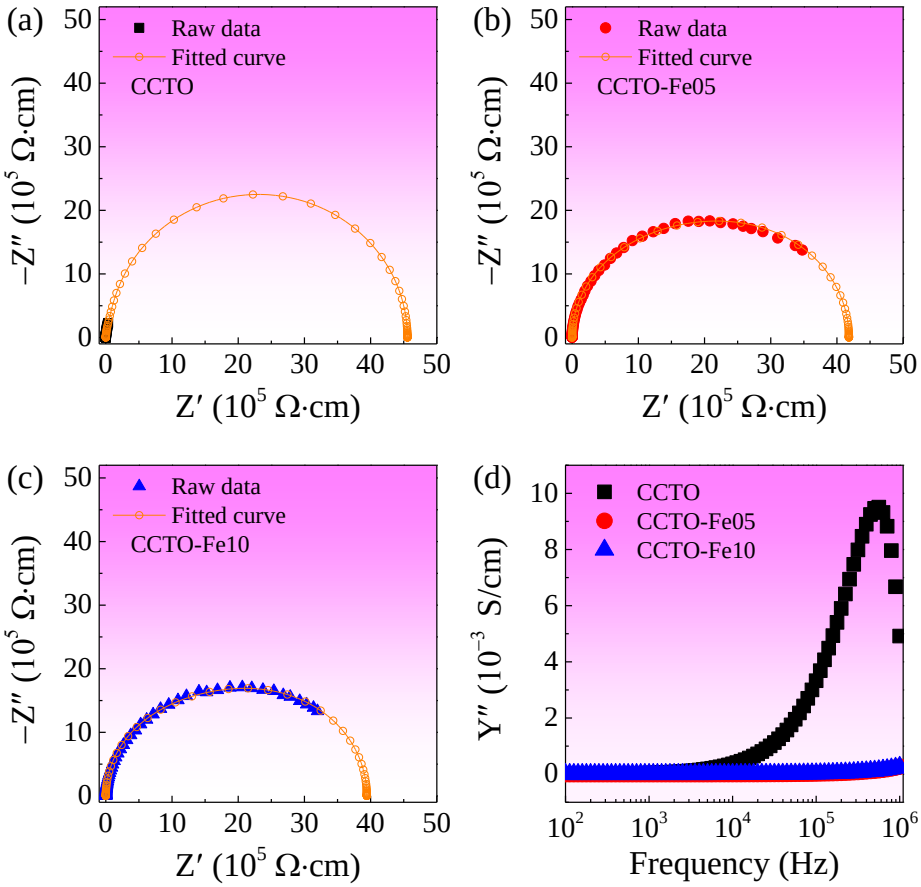

Figure 6. (a-c) Impedance complex plots at room temperature for CCTO, CCTO-Fe05, and CCTO-Fe10 ceramics, respectively. (d) Frequency dependence of Y″ of these samples.

The Z* plots for CCTO, CCTO-Fe05, and CCTO-Fe10 ceramics at room temperature are illustrated in Figures 6(a-c). These figures show that the Z* plot for CCTO ceramic does not exhibit a semicircle arc at room temperature. In contrast, the Z* plots for CCTO-Fe05 and CCTO-Fe10 ceramics display distinct semicircle arcs. These semicircle arcs indicate the electrical response of the grain boundaries. Furthermore, as shown in Figure 3(b), the rapid decrease in the tanδ values within the frequency range of 10^2 to 10^4 Hz is likely attributed to grain boundary relaxation [14, 32], which typically occurs at very low frequencies. However, in the case of Fe^{3+} doped CCTO, the presence of Fe^{3+} facilitates grain boundary relaxation at higher frequencies. To estimate the R_{gb} values for each sample, we fitted the Z* spectra using the EIS spectrum analyzer software, employing an

ideal equivalent circuit consisting of two parallel RC elements. The orange circular symbols represent the fitted spectra. R_{gb} of CCTO, CCTO-Fe05, and CCTO-Fe10 ceramics are 4.50×10^6, 3.66×10^6 and 3.38×10^6 Ω·cm, respectively. It can be observed that doping Fe^{2+} into the CCTO lattice results in a slight decrease in the R_{gb} value of the material. However, Figure 5 shows a corresponding increase in the E_b value as Fe^{3+} doping increases. This suggests that the higher internal grain resistance in CCTO-Fe05 and CCTO-Fe10 ceramics plays a crucial role in the observed increase in the E_b value. Figure 6(d) illustrates the frequency dependence of Y″, showing a distinct peak at room temperature for the CCTO sample, from which the R_g value, approximately 50 Ω·cm, can be calculated. In contrast, the R_g values for the CCTO-Fe05 and CCTO-Fe10 ceramics cannot be derived, as no corresponding peak is observed. This absence suggests that the R_g values for these ceramics are considerably higher [26]. As a result, the elevated R_g in CCTO-Fe05 and CCTO-Fe10 ceramics leads to a marked reduction in the ε′ value compared to that of the CCTO sample. It is commonly assumed that the high ε′ observed in the material originates from interfacial polarization, which occurs at the insulating grain boundaries situated between the semiconducting grains. This interfacial polarization is a key contributor to the overall dielectric behavior, as it enhances the ability to store the electrical energy of materials. However, the presence of insulating grains significantly impacts this phenomenon. When insulating grains dominate the structure, they hinder the formation of interfacial polarization at the grain boundaries [26]. As a result, the expected enhancement in dielectric properties diminishes, leading to a rapid decrease in the ε′ value of CCTO-Fe05 and CCTO-Fe10 ceramics. This behavior underscores the importance of grain boundary composition in determining the dielectric characteristics of the material.

4. Conclusions

In summary, the successful synthesis of Fe^{3+} doped $CaCu_3Ti_4O_{12}$ ceramics via a ball-milling oxide method has revealed substantial modifications in microstructural and dielectric properties. Incorporating Fe^{3+} ions resulted in a refined microstructure, effectively decreasing the mean grain size and influencing the dielectric permittivity. Notably, an increase in Fe^{3+} concentration from 0 to 0.1 led to a significant reduction in dielectric permittivity at room temperature, elucidating the relationship between enhanced grain resistance and diminished polarization density. Furthermore, Fe^{3+} ions induced low-frequency relaxation phenomena attributed to grain boundary effects. At elevated temperatures, the predominance of grain boundaries over grain resistance enabled complete interfacial polarization, consequently enhancing dielectric permittivity. The observed nonlinear J-E characteristics and the improved breakdown electric field, which increased from 31 to 41 V/cm, underscore the potential of Fe^{3+} doping. This study lays a foundational framework for the subsequent investigation of doping strategies to evaluate ceramic materials' performance in electronic applications.

5. Acknowledgements

The authors would like to thank the Physical Science, Faculty of Science and Digital Innovation, Thaksin University staff members for their support. Additionally, the authors are thankful to the Materials Physics Research Group students for generously contributing their time and assistance, which played a small but significant role in completing this work.

Author Contributions: Conceptualization, J.B. and P.S.; Methodology, P.D., A.C., and J.B.; Data curation, P.D., A.C., and J.B.; Resources, J.B. and P.S.; Investigation, P.D., A.C., J.B., and P.S.; Formal analysis, A.C. and M.M.; Validation, P.D., A.C., M.M., J.B., and P.S.; Writing-original draft preparation, J.B.; Writing-review and editing, J.B.; Visualization, J.B.; Funding acquisition J.B.

Funding: The Thaksin University Research Fund funded the research under Grant No. TSU66-NR008.

Conflicts of Interest: The authors declare that they have no known competing financial interests or personal relationships that could have influenced the work reported in this paper.

References

[1] Rhouma, S.; Megriche, A.; Souidi, E.; Saîd, S.; Autret-lambert, C. Improvement of the Nonlinear and Dielectric Properties of $CaCu_3Ti_4O_{12}$ Ceramics by Nickel Doping. *J. Inorg. Organomet. Polym. Mater.* **2023**, *34*, 221–234. https://doi.org/10.1007/s10904-023-02816-4

[2] Nachaithong, T.; Saengvong, P.; Sreejivungsa, K.; Srepusharawoot, P.; Thongbai, P.; Moontragoon, P. Huge permittivity with decreasing dissipation factor and humidity sensing properties of $CaCu_{2.9}Mg_{0.1}Ti_{4.2-x}Ge_xO_{12}$ ceramics. *Materialia* **2024**, *34*, 102061. https://doi.org/10.1016/j.mtla.2024.102061

[3] Li, J.Y.; Zhao, X.T.; Li, S.T.; Alim, M.A. Intrinsic and extrinsic relaxation of $CaCu_3Ti_4O_{12}$ ceramics: Effect of sintering. J. Appl. Phys. 2010, 108, 104104. https://doi.org/10.1063/1.3511444

[4] Subramanian, M.A.; Li, D.; Duan, N.; Reisner, B.A.; Sleight, A.W. High Dielectric Constant in $ACu_3Ti_4O_{12}$ and $ACu_3Ti_3FeO_{12}$ Phases. *J. Solid State Chem*. **2000**, *151*, 323–325. https://doi.org/10.1006/jssc.2000.8703

[5] Nautiyal, A.; Autret, C.; Honstettre, C.; De Almeida Didry, S.; El Amrani, M.; Roger, S.; Negulescu, B.; Ruyter, A. Local analysis of the grain and grain boundary contributions to the bulk dielectric properties of $Ca(Cu_{3-\gamma}Mg_\gamma)Ti_4O_{12}$ ceramics: Importance of the potential barrier at the grain boundary. *J. Eur. Ceram. Soc.* **2016**, *36*, 1391–1398. https://doi.org/10.1016/j.jeurceramsoc.2015.12.035

[6] Boonlakhorn, J.; Suksangrat, P.; Srepusharawoot, P. Dielectric properties of the $Ca_{0.25}Cu_{0.75-x}Al_xTiO_3$ ceramics: experimental and computational investigations. *Mater. Res. Express* **2024**, *11*, 026303. https://doi.org/10.1088/2053-1591/ad2799

[7] Mao, P.; Lu, G.; Yan, Q.; Annadi, A.; Guo, Y.; Wang, Z.; Liu, Z.; Xie, B.; Zhang, L. Electrodes influence on the characterization of the electrical properties of colossal permittivity $CaCu_3Ti_4O_{12}$ ceramics. *Ceram. Int*. **2022**, *48*, 32156–32163. https://doi.org/10.1016/j.ceramint.2022.07.157

[8] Wu, K.; Huang, Y.; Li, J.; Li, S. Space charge polarization modulated instability of low frequency permittivity in $CaCu_3Ti_4O_{12}$ ceramics. *Appl. Phys. Lett*. **2017**, *111*, 042902. https://doi.org/10.1063/1.4995968

[9] Sinclair, D.C.; Adams, T.B.; Morrison, F.D.; West, A.R. $CaCu_3Ti_4O_{12}$: One-step internal barrier layer capacitor. *Appl. Phys. Lett*. **2002**, *80*, 2153–2155. https://doi.org/10.1063/1.1463211

[10] Lv, Y.; Zhang, J.; Li, P.; Deng, T.; Nan, Y.; Lei, Z.; Li, Y.; Li, L. Microstructure and dielectric properties of Na and Ni co-substituted $CaCu_3Ti_4O_{12}$ ceramics with high dielectric constant and low loss. *Mater. Chem. Phys*. **2024**, *315*, 128973. https://doi.org/10.1016/j.matchemphys.2024.128973

[11] Tsyganov, A.; Morozova, N.; Vikulova, M.; Asmolova, A.; Zotov, I.; Bainyashev, A.; Gorokhovsky, A.; Gorshkov, N. Thermal behavior of La^{3+}, Ni^{2+} and Sn^{4+} co-doped $CaCu_3Ti_4O_{12}$ ceramics dielectric response. *Inorg. Chem. Commun*. **2024**, *160*, 111914. https://doi.org/10.1016/j.inoche.2023.111914

[12] Zhang, J.; Deng, T.; Li, P.; Lv, Y.; Nan, Y.; Lei, Z.; Li, Y.; Li, L. Enhanced breakdown strength and dielectric loss of $Ca_{1-3x/2}Eu_xCu_3Ti_4O_{12}$ ceramics prepared by polymer pyrolysis. *J. Mater. Sci.: Mater. Electron*. **2024**, *35*, 246. https://doi.org/10.1007/s10854-024-12001-z

[13] Xue, R.; Zhao, L.; Liu, X.; Wang, H.; Zhu, X.; Xiao, Y.; Yuan, C.; Cao, B.; Chen, Z.; Li, T.; Dai, H. Enhanced optical, dielectric, and non-Ohmic properties in Ta-doped $Bi_{2/3}Cu_3Ti_4O_{12}$ ceramics. *Solid State Sci*. **2024**, *150*, 107495. https://doi.org/10.1016/j.solidstatesciences.2024.107495

[14] Ni, L.; Chen, X.M. Enhanced giant dielectric response in Mg-substituted $CaCu_3Ti_4O_{12}$ ceramics. *Solid State Commun*. 2009, *149*, 379–383. https://doi.org/10.1016/j.ssc.2008.12.016

[15] Boonlakhorn, J.; Chanlek, N.; Krongsuk, S.; Thongbai, P.; Srepusharawoot, P. Giant dielectric properties of Mg doped $CaCu_3Ti_4O_{12}$ fabricated using a chemical combustion method: theoretical and experimental approaches. *Mater. Res. Bull*. **2022**, *150*, 111749. https://doi.org/10.1016/j.materresbull.2022.111749

[16] Peng, Z.; Li, J.; Liang, P.; Yang, Z.; Chao, X. Improved dielectric properties and grain boundary response of $SrTiO_3$ doped $Y_{2/3}Cu_3Ti_4O_{12}$ ceramics fabricated by Sol-gel process for high-energy-density storage applications. *J. Eur. Ceram. Soc*. **2017**, *37*, 4637–4644. https://doi.org/10.1016/j.jeurceramsoc.2017.06.025

[17] Li, W.; Schwartz, R.W. ac conductivity relaxation processes in $CaCu_3Ti_4O_{12}$ ceramics: Grain boundary and domain boundary effects. *Appl. Phys. Lett*. **2006**, *89*, 242906. https://doi.org/10.1063/1.2405382

[18] Ivanov, M.S.; Amaral, F.; Khomchenko, V.A.; Paixão, J.A.; Costa, L.C. Investigation of micro- and nanoscale barrier layer capacitance mechanisms of conductivity in $CaCu_3Ti_4O_{12}$ via scanning probe microscopy technique. *RSC Adv*. **2017**, 7, 40695–40704. https://doi.org/10.1039/C7RA06385G

[19] Boonlakhorn, J.; Prachamon, J.; Manyam, J.; Krongsuk, S.; Thongbai, P.; Srepusharawoot, P. Colossal dielectric permittivity, reduced loss tangent and the microstructure of $Ca_{1-x}Cd_xCu_3Ti_4O_{12-2y}F_{2y}$ ceramics. *RSC Adv*. **2021**, *11*, 16396–16403. https://doi.org/10.1039/D1RA02707G

[20] Boonlakhorn, J.; Thongbai, P.; Putasaeng, B.; Kidkhunthod, P.; Maensiri, S.; Chindaprasirt, P. Microstructural evolution, non-Ohmic properties, and giant dielectric response in $CaCu_3Ti_{4-x}Ge_xO_{12}$ ceramics. *J. Am. Ceram. Soc.* **2017**, *100*, 3478–3487. https://doi.org/10.1111/jace.14886

[21] Boonlakhorn, J.; Chanlek, N.; Srepusharawoot, P.; Thongbai, P. Controlling microstructure and significantly increased dielectric permittivity with largely reduced dielectric loss in $CaCu_{3-x}Ge_xTi_4O_{12}$ ceramics. *Appl. Phys. A* **2020**, *126*, 897. https://doi.org/10.1007/s00339-020-04069-1

[22] Boonlakhorn, J.; Chanlek, N.; Srepusharawoot, P.; Thongbai, P. Improved dielectric properties of $CaCu_{3-x}Sn_xTi_4O_{12}$ ceramics with high permittivity and reduced loss tangent. *J. Mater. Sci.: Mater. Electron*. **2020**, *31*, 15599–15607. https://doi.org/10.1007/s10854-020-04123-x

[23] Boonlakhorn, J.; Thongbai, P. Dielectric properties, nonlinear electrical response and microstructural evolution of $CaCu_3Ti_{4-x}Sn_xO_{12}$ ceramics prepared by a double ball-milling process. *Ceram. Int.* **2020**, *46*, 4952–4958. https://doi.org/10.1016/j.ceramint.2019.10.233

[24] Shannon, R.D. Revised effective ionic radii and systematic studies of interatomic distances in halides and chalcogenides. *Acta Crystallogr., Sect. A* **1976**, 32, 751–767. https://doi.org/10.1107/S0567739476001551

[25] Zhuk, N.A.; Lutoev, V.P.; Lysyuk, A.Y.; Makeev, B.A.; Belyy, V.A.; Nekipelov, S.V.; Sivkov, V.N.; Koroleva, A.V.; Krzhizhanovskaya, M.G.; Beznosikov, D.S. Thermal behavior, magnetic properties, ESR, XPS, Mössbauer and NEXAFS study of Fe-doped $CaCu_3Ti_4O_{12}$ ceramics. *J. Alloys Compd*. **2021**, *855*, 157400. https://doi.org/10.1016/j.jallcom.2020.157400

[26] Mu, C.; Zhang, H.; He, Y.; Liu, P. Influence of temperature on dielectric properties of Fe-doped $CaCu_3Ti_4O_{12}$ ceramics. *Physica B Condens. Matter* **2010**, *405*, 386–389. https://doi.org/10.1016/j.physb.2009.08.093

[27] Rai, A.K.; Singh, N.K.; Lee, S.-K.; Mandal, K.D.; Kumar, D.; Parkash, O. Dielectric properties of iron doped calcium copper titanate, $CaCu_{2.9}Fe_{0.1}Ti_4O_{12}$. *J. Alloys Compd*. **2011**, *509*, 8901–8906. https://doi.org/10.1016/j.jallcom.2011.06.008

[28] Zhuk, N.A.; Krzhizhanovskaya, M.G.; Sekushin, N.A.; Kharton, V.V.; Koksharova, L.A. Thermal expansion and electrical properties of Fe-doped $CaCu_3Ti_4O_{12}$ ceramics. *Mater. Chem. Phys*. **2020**, *258*, 123996. https://doi.org/10.1016/j.matchemphys.2020.123996

[29] Cahn, J.W. The impurity-drag effect in grain boundary motion. *Acta Metallurgica* **1962**, *10*, 789–798. https://doi.org/10.1016/0001-6160(62)90092-5

[30] Wu, K.; Huang, Y.; Hou, L.; Tang, Z.; Li, J.; Li, S. Effects of dc bias on dielectric relaxations in $CaCu_3Ti_4O_{12}$ ceramics. *J. Mater. Sci.: Mater. Electron*. **2018**, *29*, 4488–4494. https://doi.org/10.1007/s10854-017-8396-y

[31] Mao, P.; Sun, J.; Guo, Y.; Li, W.; Xiao, P.; Gerhard, M.S.; Liu, Z.; Xie, B.; Zhang, L. Giant permittivity response and enhanced nonlinear electrical properties in a novel perovskite-like ceramic with multiple elements. *Ceram. Int.* **2024**, *50*, 22501–22513. https://doi.org/10.1016/j.ceramint.2024.03.352

[32] Ni, L.; Fu, M.; Zhang, Y. Dielectric relaxation and relevant mechanism in giant dielectric constant $Sm_{2/3}Cu_3Ti_4O_{12}$ ceramics. *J. Mater. Sci.: Mater. Electron*. **2018**, *29*, 17737–17742. https://doi.org/10.1007/s10854-018-9880-8